AIP Journal of Applied Physics

Coherent A 1 g and E g phonons of antimony

Kunie Ishioka, Masahiro Kitajima, and Oleg V. Misochko

Citation: Journal of Applied Physics **103**, 123505 (2008); doi: 10.1063/1.2940130
View online: http://dx.doi.org/10.1063/1.2940130
View Table of Contents: http://scitation.aip.org/content/aip/journal/jap/103/12?ver=pdfcov
Published by the AIP Publishing

Coherent A_{1g} and E_g phonons of antimony

Kunie Ishioka,[1,a)] Masahiro Kitajima,[1] and Oleg V. Misochko[2]
[1]*Advanced Nano-Characterization Center, National Institute for Materials Science, Tsukuba, 305-0047 Japan*
[2]*Institute of Solid State Physics, Russian Academy of Sciences, 142432 Chernogolovka, Moscow Region, Russia*

(Received 18 January 2008; accepted 13 April 2008; published online 16 June 2008)

We report the ultrafast dynamics of the coherent A_{1g} and E_g phonons of antimony as a function of temperature and optical polarization. Like in bismuth, the two phonon modes exhibit nearly $\pi/2$ difference in their initial phase, suggesting their different coupling strengths with photoexcited electrons. The dependence of the phonon amplitude on the optical polarization and temperature indicates the generation of the coherent A_{1g} phonons through both displacive and Raman processes, rather than a purely displacive one. In contrast, the generation of the coherent E_g phonons can be understood within Raman framework alone. © *2008 American Institute of Physics*.
[DOI: 10.1063/1.2940130]

I. INTRODUCTION

Coherent optical phonons are the lattice atoms vibrating in phase to each other over a macroscopic spatial region. They are generated by shining femtosecond light pulses on solid crystals and observed as a terahertz (THz) modulation of the optical properties. Early experiments revealed a number of discrepancies, e.g., symmetry restrictions for generation and different initial phases, between transparent (nonabsorbing) and opaque (absorbing) materials, which stimulated the development of phenomenological generation models. Displacive excitation of coherent phonons (DECP)[1] was proposed for the totally symmetric modes in opaque materials. In this model, electronic excitation leads to a sudden change in the free energy of the lattice, and the lattice starts to oscillate around the new equilibrium position. The nuclear motion therefore follows a cosine function of time (maximum amplitude at $t=0$). Coherent phonon generation via transient depletion field screening (TDFS) in polar semiconductors[2] can be considered as its variant. Impulsive stimulated Raman scattering (ISRS) in transparent materials, by contrast, leads to a sine motion (zero amplitude at $t=0$), for the atoms oscillate around the unshifted equilibrium position of the ground state.[3]

Since the lattice interacts with light only through electrons, both DECP and ISRS mechanisms should rely on the electron-phonon ($e-p$) coupling (e.g., deformation potential and Fröhlich interactions) in the material. Distinction between the two generation models lies solely in the nature of electronic excitation, whether real or virtual. In this context, DECP was later proposed to be a resonant case of ISRS[4,5] based on the concept that the Raman scattering efficiency is represented by a complex function of photon energy.[6] However, this original resonant ISRS model with an infinite electronic lifetime failed to explain, for example, different initial phases for different coherent phonon modes in the same crystal.[7] More recently, the resonant ISRS model was modified to include finite electronic lifetime[8] to have more flexibility to reproduce the experimental observations.

In the present study, we report on the dynamics of coherent optical phonons of two different symmetries in antimony (Sb), following our previous study on bismuth (Bi).[7] Sb, like the same group element Bi, has an $A7$ crystalline structure, a rhombohedrally distorted variant of a cubic primitive structure. The distortion from cubic to rhombohedral is a Peierls distortion in which pairing the neighboring layers opens a pseudogap near the Fermi level.[9] $A7$ structure crystals sustain two Raman active optical phonons of A_{1g} and E_g symmetries. The totally symmetric A_{1g} mode is the Peierls distortion mode parallel to the trigonal axis, while the doubly degenerate E_g mode is perpendicular to the trigonal axis. Up to now, the ultrafast lattice dynamics in Sb was studied only at room temperature and primarily on the totally symmetric mode;[4,5,10,11] the generation mechanism of the coherent E_g phonon in Sb has no unique interpretation yet. We perform a systematic study on coherent phonon dynamics as a function of temperature and optical polarization. Our results indicate that, whereas ISRS contributes to the generation of both Raman active coherent phonons, only the A_{1g} mode has such a strong coupling with photoexcited electrons, which leads to a predominantly displacive generation.

II. EXPERIMENT

Single crystal Sb samples with the (0001) and $(0\bar{1}11)$ surfaces are mounted in a closed-cycle cryostat, both with the $[11\bar{2}0]$ axis in the vertical direction. Pump-probe reflectivity measurements are performed using ultrashort laser pulses with 60 fs duration, 800 nm wavelength, and 86 MHz repetition rate. Sb has a complicated band structure near the Fermi level,[12] which would allow vertical transitions with 1.55 eV photons at many different points in the Brillouin zone, as shown in Fig. 1. A plano-convex lens focuses the linearly polarized pump and probe beams to a 30 μm spot on the sample with angles of $<5°$ and 15° from the surface normal, respectively. Pump power is varied between 10 and

a)Electronic mail: ishioka.kunia@nims.go.jp

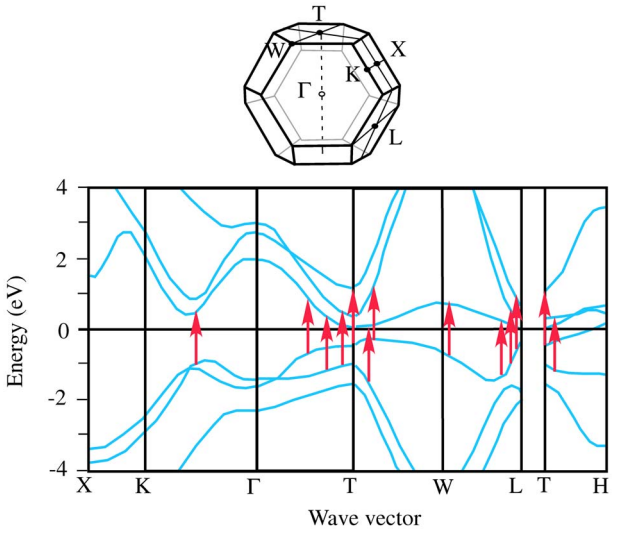

FIG. 1. (Color online) Schematic illustration of the Brillouin zone and the band structure of Sb near the Fermi level (Ref. 12). Arrows indicate energetically possible transitions with a 1.55 eV photon.

70 mW (pulse fluence of 16–115 $\mu J/cm^2$), while probe power is kept below 5 mW. The pump beam is modulated at 1.98 kHz with an optical chopper for a lock-in detection. Time delay t between the pump and probe pulses is scanned by a translational stage (slow scan).

Isotropic reflectivity ($\Delta R/R$) measurements can monitor both the symmetric (A_{1g}) and nonsymmetric (E_g) phonons, as well as mostly isotropic photoexcited electron-hole ($e-h$) pairs. In this polarization scheme, the incident probe beam is horizontally polarized (p-polarization) and is detected with a PIN detector after reflection from the sample. The difference between the signal (probe after sample) and the reference (before sample) is preamplified and recorded to cancel the fluctuation in the laser power and to enable an amplification of the small change in the reflectivity (typically $\Delta R/R \sim 10^{-5}$). Because the signal due to the E_g phonon is often obscured by the much larger isotropic signal from the A_{1g} phonon in the isotropic reflectivity, the anisotropic reflectivity $[\Delta R_{eo}/R=(\Delta R_p-\Delta R_s)/R]$ is also measured to remove the isotropic components of the reflectivity change. In this scheme, the incident probe beam is polarized 45° with respect to the optical plane. After reflection from the sample, the probe beam is analyzed into p- and s-polarized components and detected with the matched photodiodes.

III. RESULTS AND DISCUSSION

A. Polarization dependence of phonon amplitude

The isotropic reflectivity change of Sb, shown in Fig. 2(a), consists of nonoscillatory and oscillatory contributions:

$$\Delta R = \Delta R_{nonosc} + \Delta R_{osc} \approx \frac{\partial R}{\partial n} n(t) + \frac{\partial R}{\partial T_e} \Delta T_e(t) + \frac{\partial R}{\partial \chi}\frac{\partial \chi}{\partial Q} Q(t). \quad (1)$$

The nonoscillatory part ΔR_{nonosc} is dominated by the photoexcitation of $e-h$ plasma (arrows in Fig. 1) and their relaxation via intra- and intervalley scattering. It can be described

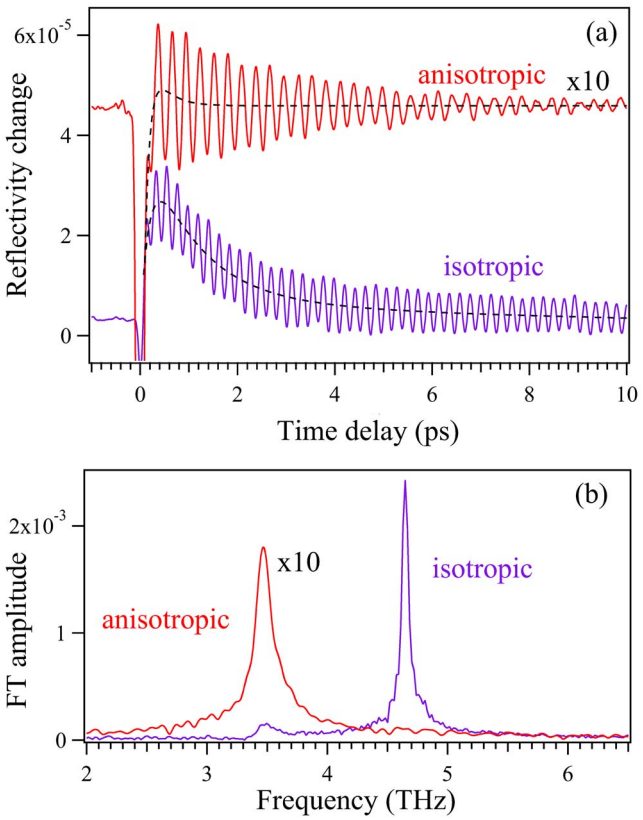

FIG. 2. (Color online) (a) Isotropic and anisotropic reflectivity changes, and (b) the Fourier transformed (FT) spectra of their oscillatory component, of Sb (0001) at 8 K under 30 mW excitation. Pump polarization is parallel to the $[11\bar{2}0]$ axis of the crystal. Broken curves in (a) indicate the nonoscillatory component of the reflectivity change due to photoexcitation and relaxation of $e-h$ pairs.

as a linear function of the excited electron density $n(t)$ and the electronic temperature change $\Delta T_e(t)$.[1] For $t \gtrsim 100$ fs it is reasonably reproduced by a double exponential function of time:

$$\frac{\Delta R_{nonosc}}{R} \approx -f_1 \exp(-\gamma_1 t) + f_2 \exp(-\gamma_2 t), \quad (2)$$

with positive constants f_1, f_2 and phenomenological rise and decay rates $\gamma_1=6.6$ ps^{-1} and $\gamma_2=0.62$ ps^{-1}. The latter is in good agreement with the $e-p$ scattering rate obtained from an electrical measurement at 10 K.[13] The oscillation in the reflectivity is induced by the coherent nuclear motion of displacement $Q(t)$ through the susceptibility χ. Fourier transformed (FT) spectrum of the oscillatory part, which is obtained by subtracting the nonoscillatory part [Eq. (2)] from the measured reflectivity change, reveals that it is mainly contributed by the A_{1g} mode at 4.6 THz but has a small E_g contribution at 3.5 THz, as shown in Fig. 2(b). The oscillatory part of the reflectivity is well described by a double damped harmonic function:

$$\frac{\Delta R_{osc}}{R} = g_a \exp(-\Gamma_a t)\sin(2\pi\nu_a t + \delta_a) + g_e \exp(-\Gamma_e t)\sin(2\pi\nu_e t + \delta_e), \quad (3)$$

where Γ, ν, and δ are the dephasing rate, the frequency, and

TABLE I. Dephasing rate Γ, frequency ν, and initial phase δ of the coherent A_{1g} and E_g phonons of Sb of 8 K, together with the electronic decay rate γ (see text). The initial phase predicted by Eq. (5) is also listed as δ_{RSFL}. Errors smaller than the last digit are not indicated.

Mode	Γ (ps^{-1})	ν (THz)	δ (deg)	γ (ps^{-1})	δ_{RSFL} (deg)
A_{1g}	0.092	4.65	-98 ± 11	0.62 ± 0.02	91
E_g	0.310 ± 0.003	3.47	-7 ± 9	3.2 ± 2.3	97 ± 6

the initial phase of the coherent phonons, with the subscripts a and e denoting A_{1g} and E_g modes, respectively.

The anisotropic reflectivity change $\Delta R_{eo}/R$, shown also in Fig. 2(a), is contributed almost exclusively by the coherent E_g phonon, enabling one to extract the dynamics of the nonsymmetric phonon with high precision. It has a very small nonoscillatory component, which is ascribed to the anisotropy in the photoexcited $e-h$ pairs[8] and can be approximated by a double exponential function with $\gamma_1=9.5$ ps^{-1} and $\gamma_2=3.2$ ps^{-1}. The insignificance of the nonoscillatory component indicates that, even though $e-h$ pairs may be photoexcited anisotropically at $t=0$, they get redistributed isotropically within the time resolution of the present experiment ($\lesssim$100 fs).

With increasing pump power, the amplitudes of the reflectivity modulation (g_a and g_e) are increased linearly. This means, according to Eq. (1), that the amplitude of the coherent nuclear motion is proportional to the photoexcitation density. The dephasing rates (Γ_a and Γ_e), frequencies (ν_a and ν_e), and initial phases (δ_a and δ_e) of the A_{1g} and E_g phonons are independent of the pump power under moderate photoexcitation in the present study and are summarized in Table I.

Experimental distinction between the impulsive and displacive generations can be primarily given by the optical polarization dependence. Coherent phonons driven by DECP should follow the polarization dependence of the optical absorption (first order process). Those driven by Raman scattering (second order process) should follow the symmetry of the Raman tensor. Though this strategy works well for a nonsymmetric phonon mode,[14] the distinction is less evident for a symmetric mode, because both absorption and the Raman tensor are isotropic on the basal plane. To avoid the controversy, we measure the polarization dependence on low-symmetry crystallographic surface. Measurements on the $(0\bar{1}11)$ surface of $A7$ crystals allow probing all the components of the Raman tensors of the A_{1g} and E_g phonons:

$$R_a=\begin{pmatrix} a & 0 & 0 \\ 0 & a & 0 \\ 0 & 0 & b \end{pmatrix}$$

and

$$R_e=\begin{pmatrix} c & 0 & 0 \\ 0 & -c & d \\ 0 & d & 0 \end{pmatrix},\begin{pmatrix} 0 & -c & -d \\ -c & 0 & 0 \\ -d & 0 & 0 \end{pmatrix}. \quad (4)$$

Since the absorption of 800 nm light by Sb is isotropic,[15] the amplitude of the A_{1g} phonon from the $(0\bar{1}11)$ surface should

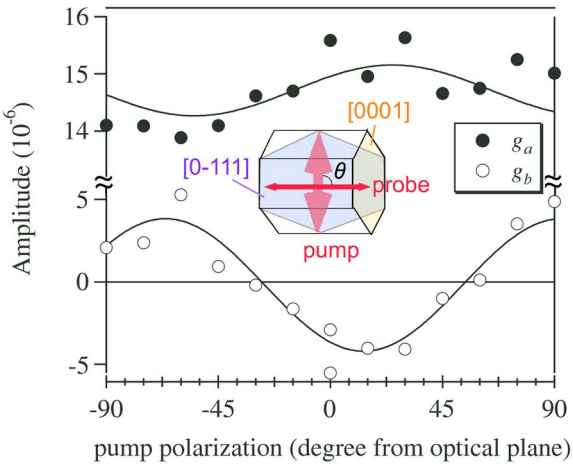

FIG. 3. (Color online) Pump-polarization dependence of g_a and g_e obtained from isotropic reflectivity measurements on the Sb $(0\bar{1}11)$ surface with pump power of 30 mW at 8 K. Inset illustrates schematically the surface and the polarizations of the pump and probe. Solid curves represent fitting with $\cos 2\theta$ with polarization angle θ.

be independent of the optical polarization if it is a purely displacive process. The result, plotted in Fig. 3, shows a clear angle dependence of g_a, indicating that the Raman tensor is involved in the generation of the coherent A_{1g} phonon. We note that, however, this does not automatically exclude DECP contribution. For compound semiconductors, for example, two different generation mechanisms, TDFS and ISRS, can contribute to excitation of a single phonon mode.[14,16]

B. Initial phase of coherent phonon

Initial phases of coherent phonons were also used for experimental distinction between the generation mechanisms, though the interpretation was controversial. Figure 4 shows the reflectivity changes in the early delay times to compare the initial phases δ_a and δ_e. The isotropic reflectivity gives δ_a very close to $-\pi/2$ [Figs. 4(a) and 4(b)], while the anisotropic reflectivity of the (0001) surface reveals that δ_e is nearly zero [Fig. 4(c)]. Similar phase difference between the A_{1g} and E_g phonons was also observed in the previous studies on Sb (Ref. 4) and Bi.[7]

The observed $\pi/2$ phase difference can be a touchstone of generation models. DECP assumes a cosine-like nuclear motion on the excited electronic state,[1] while (nonresonant) ISRS assumes a sine-like motion on the ground state.[3] In this simple framework, the phase difference would be interpreted that A_{1g} and E_g phonons oscillate on the excited and the ground states, respectively. Such a paradoxical interpretation can be paraphrased as follows, based on a recent theoretical simulation on Bi.[17] The potential energy surface along the trigonal axis is significantly affected by an electronic excitation, because the motion along the axis (A_{1g}) is the Peierls distortion mode. The strong coupling between the A_{1g} phonon and the excited electrons leads to a predominantly displacive generation of coherent A_{1g} phonon in Sb as well as in Bi.[7] In contrast, the potential energy surface perpendicular to

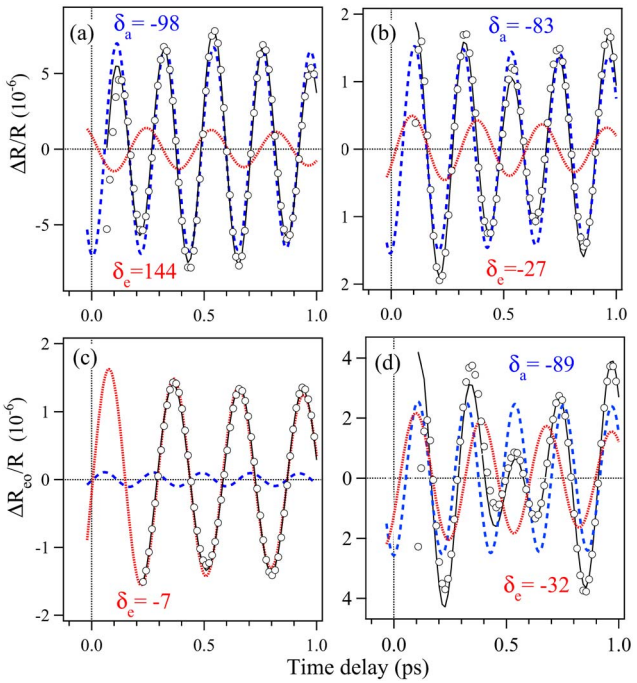

FIG. 4. (Color online) Oscillatory part of the reflectivity change of Sb at 8 K (open circles), its fit to Eq. (3) (black solid curve), and its A_{1g} and E_g components (blue broken and red dotted curves). The reflectivity change is obtained from isotropic measurements on the (0001) (a) and $(0\bar{1}11)$ surfaces (b), and from anisotropic measurements on the (0001) (c) and $(0\bar{1}11)$ surfaces (d). Initial phases obtained by fitting to Eq. (3) are shown in degrees in each panel.

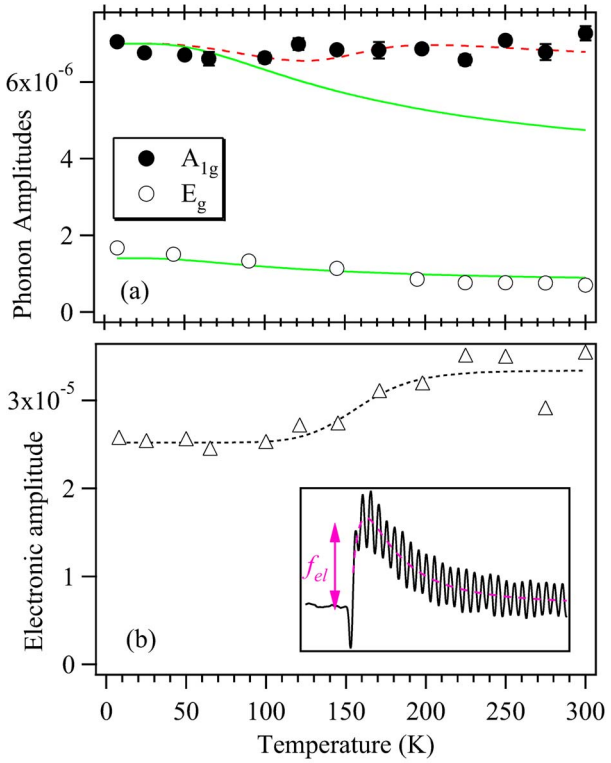

FIG. 5. (Color online) Temperature dependence of (a) the initial amplitudes of coherent A_{1g} and E_g phonons, and (b) the amplitude of the electronic transient, both obtained from isotropic reflectivity measurement on the (0001) surface of Sb. Solid curves in (a) and (b) are to guide the eye. Inset in (b) illustrates how to obtain f_{el} as the maximum height of the nonoscillatory part of the isotropic reflectivity change.

the axis, along which the E_g phonon oscillates, is little affected, leading to a negligible contribution of DECP to the nonsymmetric phonon.

The original resonant ISRS with an infinite electronic lifetime[5] cannot explain the observed $\pi/2$ difference, since the two phonon modes show very similar wavelength dependence in their Raman cross section.[18] The recently proposed "Raman scattering finite lifetime (RSFL)" model[8] is more flexible in this context, since the initial phase for a sine function of time is given as a function of γ:

$$\delta_{\mathrm{RSFL}} = \tan^{-1}\left(\frac{4\pi^2\nu^2\epsilon_1' + (\gamma-\Gamma)2\epsilon_2}{2\pi\nu(2\epsilon_2 - \gamma\epsilon_1')}\right) + \frac{\pi}{2}, \tag{5}$$

where $\epsilon=\epsilon_1+i\epsilon_2$ is the dielectric function of the material at the laser frequency ω_0, and $\epsilon_1'=d\epsilon_1/d\omega$. (Note that in Ref. 8 the phase was given for a cosine function of time.) We estimate γ for the A_{1g} and E_g modes from γ_2 of the isotropic and anisotropic reflectivity, assuming that they respectively couple with the isotropic and anisotropic component of the photoexcited electrons.[8] Equation (5) then predicts $\delta_{\mathrm{RSFL}}=91°$ and 97° for the A_{1g} and E_g modes of Sb, respectively, for ν, Γ, γ listed in Table I and ϵ_1', ϵ_2 from Ref. 8. The RSFL model reproduces the initial phase of the A_{1g} phonon reasonably, but fails to reproduce that of the E_g phonon. For Bi, the RSFL model predicts $\delta_{\mathrm{RSFL}}=90°$ for both A_{1g} and E_g phonons, again in reasonable agreement with the experimentally observed $\delta_a=-101°$ but far from $\delta_e=144°$.[7]

The difficulty in applying the RSFL model to the analysis lies largely in the ambiguity in the definition of γ, especially of its anisotropic component, which the authors of Ref. 8 assumed to couple with the nonsymmetric phonons. In the estimation above, we followed the reference and obtained the electronic decay rate for the E_{1g} phonon from the nonoscillatory part of the anisotropic reflectivity change. However, the very small nonoscillatory component is more likely to indicate that the photoexcited $e-h$ pairs lose the anisotropy significantly faster than the time resolution of the present experiment (<100 fs). Indeed, the experimental initial phase of the E_g phonon (−7°) is reproduced only by assuming $\gamma \gtrsim 100$ ps^{-1}, which is comparable to or faster than the electronic dephasing in Sb.[13] With such large γ, one may as well conclude that the coherent E_g phonon is coupled with a virtual excitation.

C. Temperature dependence of phonon amplitude

Amplitudes of coherent phonons can give an additional insight on the generation mechanism when we control an external parameter such as temperature. Figure 5(a) shows a clearly different temperature dependence between the amplitudes of the two phonon modes; g_a remains almost constant while g_e decreases monotonically with rising temperature. Interestingly, neither resembles the temperature dependence of the amplitude of the electronic transient, f_{el}, obtained from the maximum height of the nonoscillatory component in the isotropic reflectivity change [inset of Fig. 5(b)]. It increases between 100 and 200 K but remains almost constant at lower and higher temperatures, as shown in Fig. 5(b). f_{el} is often

used as a qualitative measure for the photoexcited carrier density.[19] Since the amplitude of DECP-driven coherent phonons should be proportional to the carrier density,[1] different temperature dependence between the phonic and electronic amplitudes is clearly indicative of non-DECP (i.e., Raman) contribution to the generation of the coherent A_{1g} phonons, as has been discussed based on the polarization dependence in Sec. III A.

Although the polarization dependence and the initial phase indicate a purely ISRS generation for the coherent E_g phonons, the temperature dependence of its amplitude is opposite from what is expected for a Raman scattering cross section. The cross section for a Stokes process should be proportional to the population of the initial state, which, following a Bose-Einstein distribution function, increases monotonically with temperature. By contrast, the present result suggests that the increasing population of thermal phonons hinders the generation of coherent phonons. Since the characteristic temperature of the monotonic decrease coincides roughly to the Debye temperature (210 K for Sb),[20] we tentatively explain the observed temperature dependence in terms of the increasing interaction with thermally excited incoherent phonons at higher temperature. Similar monotonic decrease of the E_g phonon amplitude around the Debye temperature was also observed for Bi (Ref. 7) and Zn.[19]

If we compare the FT spectrum of our pump-probe signal [Fig. 2(b)] with spontaneous Raman spectra in the literature,[9,21,22] we can see that the A_{1g} phonon is generated significantly more effectively in time-domain than in the Raman spectrum. Because the resonant Raman model[4,8] carries a prediction that, given the excitation wavelength, the relative intensities gained from time- and frequency-domain measurements should be the same, the discrepancy is yet further evidence that DECP is at work in generating A_{1g} phonon beside the Raman process, rather than the resonant Raman scattering alone.

IV. CONCLUSION

We have demonstrated ultrafast dynamics of the coherent A_{1g} and E_g phonons of Sb at and below room temperature. While the polarization dependence suggests that both coherent phonons have Raman contribution in their generation, their initial phases indicate that the coherent A_{1g} phonon is primarily generated via a strong coupling with the photoexcited electrons. The temperature dependence of the phonon amplitudes also support that both DECP and ISRS contribute to the generation of the totally symmetric coherent phonons, while the generation of doubly degenerate coherent phonons can be understood as purely ISRS.

ACKNOWLEDGMENTS

Support from the JSPS and RFBR (Grant Nos. 05-02-19910 and 07-02-00148) is gratefully acknowledged.

[1] H. J. Zeiger, J. Vidal, T. K. Cheng, E. P. Ippen, G. Dresselhaus, and M. S. Dresselhaus, Phys. Rev. B **45**, 768 (1992).
[2] T. Dekorsy, G. C. Cho, and H. Kurz, in *Light Scattering in Solids VIII*, edited by M. Cardona and G. Güntherodt (Springer, Berlin, 2000), Chap. 4.
[3] L. Dhar, J. A. Rogers, and K. A. Nelson, Chem. Rev. **94**, 157 (1994).
[4] G. A. Garrett, T. F. Albrecht, J. F. Whitaker, and R. Merlin, Phys. Rev. Lett. **77**, 3661 (1996).
[5] T. E. Stevens, J. Kuhl, and R. Merlin, Phys. Rev. B **65**, 144304 (2002).
[6] M. Cardona, in *Light Scattering in Solids II*, edited by M. Cardona and G. Güntherodt (Springer, Berlin, 1982), Chap. 2.
[7] K. Ishioka, M. Kitajima, and O. Misochko, J. Appl. Phys. **100**, 093501 (2006).
[8] D. M. Riffe and A. J. Sabbah, Phys. Rev. B **76**, 085207 (2007).
[9] X. Wang, K. Kunc, I. Loa, U. Schwarz, and K. Syassen, Phys. Rev. B **74**, 134305 (2006).
[10] T. K. Cheng, S. D. Brorson, A. S. Kazeroonian, J. S. Moodera, G. Dresselhaus, M. S. Dresselhaus, and E. P. Ippen, Appl. Phys. Lett. **57**, 1004 (1990).
[11] T. K. Cheng, J. Vidal, H. J. Zeiger, G. Dresselhaus, M. S. Dresselhaus, and E. P. Ippen, Appl. Phys. Lett. **59**, 1923 (1991).
[12] X. Gonze, J. P. Michenaud, and J. P. Vigneron, Phys. Rev. B **41**, 11827 (1990).
[13] J. J. Lin, L. Tsang-Jou, and T. M. Wu, Phys. Rev. B **61**, 3170 (2000).
[14] Y. M. Chang, Appl. Phys. Lett. **82**, 1781 (2003); Y. M. Chang, *ibid.* **85**, 5224 (2004).
[15] A. P. Lenham, D. M. Treherne, and R. J. Metcalfe, J. Opt. Soc. Am. **55**, 1072 (1965).
[16] K. Ishioka, M. Kitajima, J. Irisawa, Y. Hironaka, K. Ushida, and K. Nakamura, Jpn. J. Appl. Phys., Part 1 **45**, 9111 (2006).
[17] E. S. Zijlstra, L. L. Tatarinova, and M. E. Garcia, Phys. Rev. B **74**, 220301 (2006).
[18] J. B. Renucci, W. Richter, M. Cardona and E. Schönherr, Phys. Status Solidi B **60**, 299 (1973).
[19] M. Hase, K. Ishioka, J. Demsar, K. Ushida, and M. Kitajima, Phys. Rev. B **71**, 184301 (2005).
[20] G. K. White, J. Phys. C **5**, 2731 (1972).
[21] M. L. Bansal and A. P. Roy, Phys. Rev. B **33**, 1526 (1986).
[22] P. S. Pizani, C. E. M. Campos, and P. Puech, Appl. Phys. Lett. **77**, 2924 (2000).